Chemical Science

ROYAL SOCIETY OF CHEMISTRY

EDGE ARTICLE

View Article Online
View Journal

Check for updates

Cite this: DOI: 10.1039/d5sc04298d

All publication charges for this article have been paid for by the Royal Society of Chemistry

Open Access Article. Published on 24 July 2025. Downloaded on 8/11/2025 11:25:40 AM. This article is licensed under a Creative Commons Attribution-NonCommercial 3.0 Unported Licence.

# Single solvent molecule effect over $S_N2$ and E2 competition in the hydroperoxide anion reaction with ethyl-iodide†

Xiangyu Wu, [a] Chongqin Zhu, [b] Joseph S. Francisco *[c] and Jing Xie *[a]

The influence of individual solvent molecules on the dynamics of competing reactions remains largely unexplored for many important chemical systems. Herein, direct dynamics simulations revealed that a single water molecule has multifaceted effects on the reaction between the hydroperoxide anion $HOO^-$ and $C_2H_5I$. The introduction of one water reduced the overall reaction rate and shifted the preference from elimination (E2) to substitution ($S_N2$) reactions because of the differential solvation effect. Increasing the collision energy lowered the overall reactivity but did not change the $S_N2$-to-E2 pathway ratio. Notably, the additional water molecules also induced new competing pathways that used $HO^-$ as an attacking nucleophile *via* proton transfer within the nucleophile $HOO^-(H_2O)$; here, both the $HO^-$-E2 and $HO^-$-$S_N2$ trajectories were observed at small percentages. The occurrence of the $HO^-$ paths was driven by the extensive proton transfer within the pre-reaction complex well, but was suppressed by the entropy effect and increased barriers. In addition, water molecules complicated the reaction mechanisms, increased the percentage of indirect mechanisms, and affected the dynamic features of proton transfer. As in the solvent-free system, protons were frequently exchanged between the nucleophiles and substrates, whereas in the singly solvated system, proton exchange mainly occurred within the nucleophiles. This work highlights the dynamic role of solvent molecules and may have profound impacts on reaction dynamics, with relevance to organic synthesis and chemistry in biosystems, microdroplets, and aerosols.

Received 12th June 2025
Accepted 23rd July 2025

DOI: 10.1039/d5sc04298d

rsc.li/chemical-science

## Introduction

In addition to providing a liquid-phase reaction environment, solvents have a profound impact on chemical reactions, such as affecting the reaction kinetics through catalysis[1–5] or inhibition,[6] altering the product branching ratios,[7–9] and modifying the reaction dynamics.[4,10,11] The influence of the individual solvent molecules on the reaction dynamics has long been a central topic among experimental and theoretical researchers in the fields of atmospheric, physical, and interfacial chemistry.[1,3,6,7,9,12–19] In particular, the development of crossed-beam imaging experimental techniques and computational simulation powers enables a detailed investigation of the reaction mechanisms and dynamics.[10,20–29] Ion–molecule reactions represent a prevalent category of chemical reactions and can potentially be affected by solvent effects.[10,30–32] However, the dynamic and steric effects caused by the individual solvent molecules remain elusive for numerous critical ion-molecule reactions.

The hydroperoxide anion ($HOO^-$), which is the conjugate base of hydrogen peroxide (HOOH), is an important species across diverse fields. For example, in atmospheric chemistry, $HOO^-$ participates in reactions that contribute to acid rain formation and ozone consumption.[33] In the cellular biology field, $HOO^-$ is involved in the oxidative processes linked to ageing and degenerative diseases since it reacts with lipids and proteins.[34–37] Industrially, $HOO^-$ serves as a key oxidant in semiconductor cleaning processes and peroxide bleaching, where it facilitates the breakdown of chromophores to decolorize fabrics.[38–40] Additionally, $HOO^-$ likely participates in

[a]Key Laboratory of Cluster Science of Ministry of Education, School of Chemistry and Chemical Engineering, Beijing Institute of Technology, Beijing 100081, China. E-mail: jingxie@bit.edu.cn

[b]Key Laboratory of Theoretical and Computational Photochemistry, Ministry of Education, College of Chemistry, Beijing Normal University, Beijing 100875, China

[c]Department of Earth and Environmental Science and Department of Chemistry, University of Pennsylvania, Philadelphia, Pennsylvania 19104, USA. E-mail: frjoseph@sas.upenn.edu

† Electronic supplementary information (ESI) available: Direct rebound mechanism of the $HOO^-$-$S_N2$ path (Video S1); direct stripping mechanism of the $HOO^-$-$S_N2$ path (Video S2); direct rebound mechanism of the $HOO^-$-E2 path (Video S3); direct stripping mechanism of the $HOO^-$-E2 path (Video S4); indirect mechanism, roundabout mechanism of the $HOO^-$-$S_N2$ path (Video S5); indirect mechanism of the H-exchange of the $HOO^-$-$S_N2$ path (Video S6); indirect mechanism of the $HOO^-$-*anti*-E2 path (Video S7); indirect mechanism of the $HOO^-$-*syn*-E2 path (Video S8); indirect mechanism of the $\alpha$-elimination of the $HOO^-$-E2 path (Video S9); indirect mechanism of the $HO^-$-$S_N2$ path (Video S10); indirect mechanism of the $HO^-$-E2 path (Video S11). See DOI: https://doi.org/10.1039/d5sc04298d

Open Access Article. Published on 24 July 2025. Downloaded on 8/11/2025 11:25:40 AM. This article is licensed under a Creative Commons Attribution-NonCommercial 3.0 Unported Licence.

hydrocarbon oxidation and combustion processes, such as acetylene combustion; here, it reacts with formaldehyde and formic acid.[41,42] Recent advancements in energy storage have also highlighted its importance since shifting the discharge intermediate from superoxide $O_2^-$ to $HOO^-$ in aprotic Li–$O_2$ batteries can reduce the byproducts and overpotentials to enhance battery efficiency.[43] Due to its multifaceted roles, $HOO^-$ needs to be comprehensively understood to advance research in atmospheric science, biochemistry, industrial application, and energy technologies.

The hydrated $HOO^-$ ion has garnered great interest for its unique properties.[44–49] Microhydrated $HOO^-$ ions, $HOO^-(H_2O)_n$, can undergo proton transfer to generate isomers in the form of $HO^-(HOOH)(H_2O)_{n-1}$, where the latter is lower in energy when the number of water molecules $n$ is less than 6.[48] Hence, when hydrated $HOO^-$ ions interact with a substrate, they can behave as dual nucleophiles, similar to $CN^-$, such that either $HOO^-$ or $HO^-$ can act as nucleophiles.[50–53] Previously, direct dynamics simulations of singly hydrated $HOO^-$ reacting with $CH_3Cl$ and $CH_3I$ revealed that the $HOO^-$ path is dominant and produces $CH_3OOH$, whereas the $HO^-$ path contributes only a minor fraction of the products and produces $CH_3OH$.[32,54] Calculations have shown that increasing the degree of hydration causes the $HO^-$ path to be even less favourable.[55] Enlarging the substrate from methyl halides to ethyl halides introduces a competing reaction to the $S_N2$ pathway, namely, elimination reactions (E2).[4,9,56–58] Either $HOO^-$ or $HO^-$ can serve as the base for the E2 reaction. Interestingly, when singly hydrated $HOO^-$ reacts with ethyl halides, the E2 reaction products of the $HOO^-$ and $HO^-$ paths are identical (Scheme 1) and have similar barriers.[59] Distinguishing these two product channels by experiment is a formidable task. Therefore, the reaction dynamics need to be investigated using computational simulations.

In this work, we performed direct dynamics simulations on $CH_3CH_2I$ reacting with $HOO^-$ and $HOO^-(H_2O)$ in the gas phase to reveal the role of a single water molecule in the reaction dynamics. The key questions we explored are as follows: What is the effect of one water molecule on (1) the reaction kinetics, *i.e.*, the rate constants; (2) the competition between $S_N2$ and E2 reactions, *i.e.*, their ratio and atomic-level mechanism; and (3) the competition between the $HOO^-$ and $HO^-$ pathways? (4) What is the role of collision energy? The simulations focus on the microhydrated $HOO^-$ ions and reveal that the solvent molecules not only affect the competition between the different pathways but also influence the dynamic behaviour of chemical reactions. These findings provide valuable theoretical guidance for the environment, energy, and synthesis chemistry.

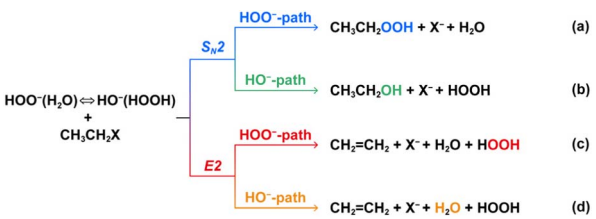


Scheme 1 $S_N2$ and E2 reaction pathways of the $HOO^-(H_2O)$ + $CH_3CH_2X$ reactions.

## Computational methods

Direct dynamics simulations were performed at the CAM-B3LYP/6-31+G(d,p)&ECP level of theory using the VENUS/NWChem program.[60–62] The 6-31+G(d,p) basis set was used for the H, C, and O atoms, and the LANL2DZdp basis set and effective core potential (ECP) were used for iodine. The choice of this method was based on the accuracy of the structure and reaction enthalpy (ESI Note and Tables S1–S3†). The initial distance between $CH_3CH_2I$ and $HOO^-$ or $HO^-(HOOH)$ was 15 Å, and the collision energy ($E_{coll}$) was 0.04 eV (equivalent to 300 K) and 1.0 eV. The vibrational and rotational temperatures of the reactants were 300 K, and the vibrational and rotational energies were sampled for their respective Boltzmann distributions. At an $E_{coll}$ of 0.04 eV, the trajectories were calculated at a fixed impact parameter $b$ of 0, 1, 3, 5, 7, 9, 11, 13, and 15 Å; here, the reaction probability was zero at the maximum $b$ under investigation, namely, $b_{max}$. At $E_{coll}$ = 1.0 eV, the impact parameter $b$ was 0, 1, 3, 5, 7, and 9 Å for the $HOO^-$ system, and $b$ was 0, 1, 3, 5, and 7 Å for the $HO^-(HOOH)$ system. For each $b$, approximately 100–120 trajectories were simulated, resulting in a total of 3178 trajectories. Considering the computational efficiency, the trajectories were integrated by the velocity Verlet method[63] with a 1.0 fs time step.

## Results and discussion

### Overall reactivity

The reactivities of $CH_3CH_2I$ with $HOO^-$ and $HO^-(HOOH)$ at collision energies of 0.04 eV and 1.0 eV were evaluated by plotting the opacity functions $P_r(b)$ *versus* the impact parameter $b$ for the total reaction and different product channels, *i.e.*, the $HOO^-$-$S_N2$, $HO^-$-$S_N2$, $HOO^-$-E2, and $HO^-$-E2 pathways (Fig. 1). In comparison, increasing the collision energy decreases both the maximum impact parameter $b_{max}$ and the reaction probability at each $b$, *i.e.*, $P_r(b)$, which together lower the overall reactivity. For example, for the unsolvated $HOO^-$ + $CH_3CH_2I$ reaction, the value of $b_{max}$ decreases from 15.0 Å at an $E_{coll}$ of 0.04 eV to 9 Å at 1.0 eV; $P_r(b)$ at $b$ = 1 Å decreases from 0.89 at 0.04 eV to 0.23 at 1.0 eV. Evaluating the total integral cross sections (ICSs) $\sigma_r$ *via* the formula $\int_0^{b_{max}} P_r(b)2\pi b\mathrm{d}b$ provides an $\sigma_r$ value of 452.8 ± 7.6 Å$^2$ at 0.04 eV and a much smaller value of 17.7 ± 1.9 Å$^2$ at 1.0 eV. The corresponding reaction rate constants of $k(E_{coll}, T_v, T_r) = v(E_{coll})\sigma(E_{coll}, T_v, T_r)$ are (23.8 ± 0.4) and (4.7 ± 0.5) × $10^{-10}$ cm$^3$ mol$^{-1}$ s$^{-1}$. These results indicate that increasing $E_{coll}$ from 0.04 to 1.0 eV reduces the rate constant by a factor of 4.

Adding one water molecule to the nucleophile barely affects the value of $b_{max}$ but lowers $P_r(b)$. For example, at $b$ = 1.0 Å and $E_{coll}$ = 0.04 eV, the total $P_r(b)$ decreases from 0.89 for the unsolvated system to 0.49 for the singly solvated system. As a result, this leads to a decrease in the cross-section and


© 2025 The Author(s). Published by the Royal Society of Chemistry

Open Access Article. Published on 24 July 2025. Downloaded on 8/11/2025 11:25:40 AM. This article is licensed under a Creative Commons Attribution-NonCommercial 3.0 Unported Licence.

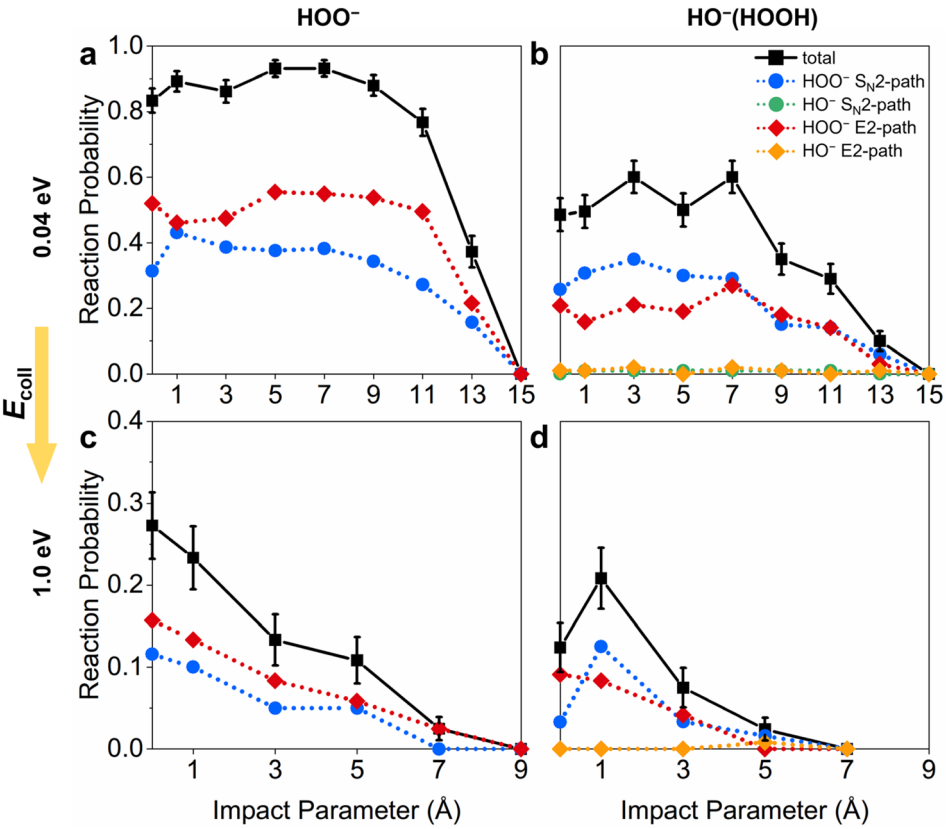


Fig. 1 Opacity functions $P_r(b)$ of the different pathways for $CH_3CH_2I$ reacting with (a and c) $HOO^-$ and (b and d) $HO^-(HOOH)$ at collision energies of 0.04 eV (top) and 1.0 eV (bottom).

reaction rate constant. For the singly solvated $HO^-(HOOH)$ + $CH_3CH_2I$ system, $\sigma_r$ is 209.2 ± 8.0 Å$^2$ at 0.04 eV and 7.5 ± 1.0 Å$^2$ at 1.0 eV, and the respective rate constants $k$ are (9.3 ± 0.4) and (1.7 ± 0.2) × $10^{-10}$ cm$^3$ mol$^{-1}$ s$^{-1}$. Taken together, adding one water to the system decreases the rate constant by factors of 1.6 and 1.8 at $E_{coll}$ of 0.04 and 1.0 eV, respectively.

## Product channels

The $S_N2$ and E2 reactions compete with each other during the reaction process. For the unsolvated system, both the $HOO^-$-$S_N2$ and the $HOO^-$-E2 pathways occur throughout the range of $b$ from 0 to $b_{max}$. Notably, the E2 pathway remains dominant over the $S_N2$ pathway at each $b$ (Fig. 1a and c). The branching ratio derived from the ICSs for E2 : $S_N2$ is 60.4 : 39.6 at 0.04 eV and 62.7 : 37.3 at 1.0 eV (Fig. 2a and c). These results show that increasing $E_{coll}$ slightly enhances the advantage of E2 over $S_N2$ reactions, even though the overall reactivity is reduced.

The addition of one water molecule to the system introduces significant changes in the products and their ratios, in addition to affecting the reactivity. At an $E_{coll}$ of 0.04 eV, in addition to the normal $HOO^-$-$S_N2$ and E2 pathways, additional pathways are observed owing to proton transfer within the nucleophile. One is the $HO^-$-$S_N2$ pathway; here, $HO^-$ behaves as the attacking nucleophile and generates $CH_3OH + H_2O_2 + I^-$, and this reaction occurs at $b$ values of 1, 3, 5, 7, 9, and 11 Å. The other is the $HO^-$-E2 pathway, which generates the same products as normal $HOO^-$-E2, *i.e.*, $C_2H_4 + H_2O_2 + H_2O + I^-$, but the attacking base is $HO^-$. This reaction occurs at $b$ values of 0, 1, 3, 7, 9 and 13 Å. However, both pathways are quite rare, where the $HO^-$-$S_N2$ and $HO^-$-E2 paths account for 2.2% and 2.6%, respectively, of the overall products. At an $E_{coll}$ of 1.0 eV, only the $HO^-$-E2 pathway is observed, with a minor contribution of 6.8%. Nevertheless, the observation of these $HO^-$-attacking trajectories highlights the unique role of water molecules in shaping the reaction dynamics.[32,54]

Furthermore, the solvated products, *i.e.*, $I^-(H_2O)$ and $I^-(HOOH)$, are observed in both the $S_N2$ and E2 reaction trajectories. Although the calculated reaction energies are more negative for the solvated products than for the separated products (Fig. S1†), the unsolvated product $I^-$ ions dominate over the solvated $I^-$(solvent) ions. In comparison, the reaction energy of the $CH_3OOH + I^-(H_2O)$ products is −47.8 kcal mol$^{-1}$, and this value is 11.4 kcal mol$^{-1}$ lower than that of the $CH_3OOH + I^- + H_2O$ products; the reaction energy of the $C_2H_4 + I^-(H_2O) + H_2O_2$ products is −22.7 kcal mol$^{-1}$, and this value is 11.4 kcal mol$^{-1}$ lower than that of the $C_2H_4 + I^- + H_2O + H_2O_2$ products. At an $E_{coll}$ of 0.04 eV, the simulated product anion ratio $I^-$ : $I^-$(solvent) is approximately 97 : 3, highlighting that solvated pathways are suppressed because of the dynamic nature of the reactions in the gas phase; these results are consistent with previous experimental and theoretical works.[8,22,30,64] When the collision energy is increased to 1.0 eV, no solvated ions are found. Halogen-bonded

Open Access Article. Published on 24 July 2025. Downloaded on 8/11/2025 11:25:40 AM.
This article is licensed under a Creative Commons Attribution-NonCommercial 3.0 Unported Licence.

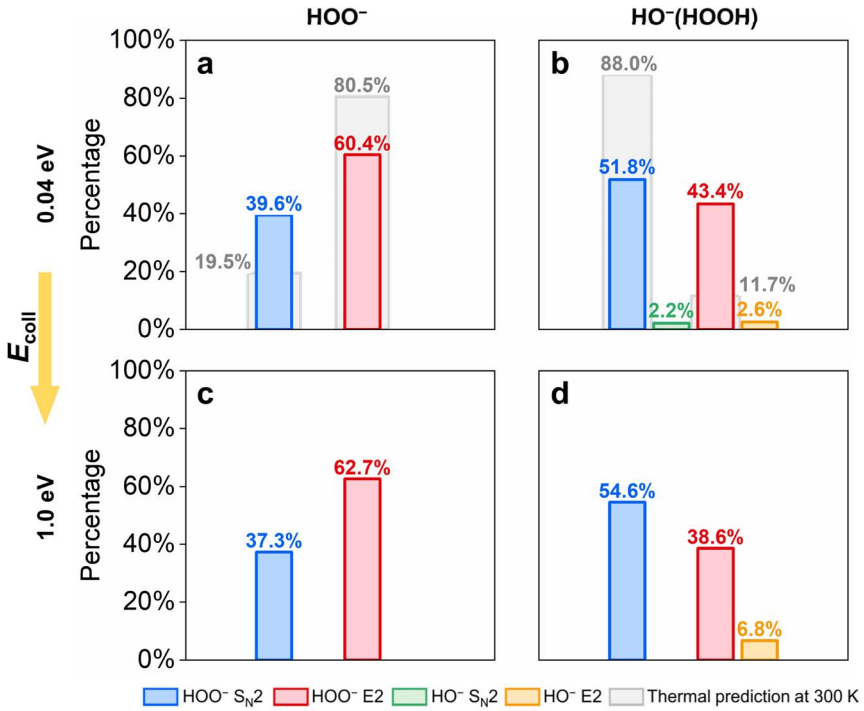


Fig. 2 Branching ratios of the $HOO^-$-$S_N2$ (blue), $HOO^-$-E2 (red), $HO^-$-$S_N2$ (green) and $HO^-$-E2 (orange) pathways for $CH_3CH_2I$ reacting with (a and c) $HOO^-$ and (b and d) $HO^-$(HOOH) at collision energies of 0.04 eV (top) and 1.0 eV (bottom).

complexes, either $[C_2H_5\cdots I\cdots OOH]^-$ or $[C_2H_5\cdots I\cdots OOH]^-(H_2O)$, are observed in both solvent-free and singly solvated systems and are less than 1%.

Moreover, the additional water molecules shift the preference between the $S_N2$ and E2 pathways compared with the solvent-free case (Fig. 2b and d). For the singly solvated system, at an $E_{coll}$ of 0.04 eV, the $HOO^-$-$S_N2$ path has a higher $P_r(b)$ than the $HOO^-$-E2 path from $b$ of 0 to 5 Å, and they have similar $P_r(b)$ values at $b$ values of 7 to 13 Å. At an $E_{coll}$ of 1.0 eV, the $HOO^-$-$S_N2$ path has a higher $P_r(b)$ at $b$ values of 1 and 5 Å. The resulting branching ratios of E2 : $S_N2$ are approximately 46 : 54 under both collision energies. Considering only the $HOO^-$ pathways, *i.e.*, excluding the $HO^-$ pathways, $S_N2$ is also preferred over E2. The phenomenon that solvent molecules promote a portion of the $S_N2$ path has also been observed in $F^-(CH_3OH) + CH_3CH_2Br$ reactions.[4,5] Why does a single water molecule shift the preference between the $S_N2$ and E2 pathways in the studied system? To answer this question, we analysed the potential energy profiles, the atomistic mechanisms and the dynamics of water molecules in the following section.

## Potential energy profiles

The potential energy profile of each $S_N2$ and E2 pathway (Fig. 3) displays a double-well shape, where a central transition state (TS) connects a shallow well of pre-reaction complex (RC) and a deep well of the postreaction complex (PC). All $S_N2$ and E2 reactions are highly exoergic, and the $S_N2$ products are more exoergic.

For the unsolvated system, both the back-side $S_N2$ pathway (denoted as a) and the *anti*-E2 pathway (denoted as c) share the same pre-reaction complex (denoted as 0aRC), with a relative energy of −18.3 kcal mol$^{-1}$ with respect to reactants $HOO^-$ + $C_2H_5I$. The relative energies of the transition states of the $S_N2$ pathway (0aTS, −17.9 kcal mol$^{-1}$) and the *anti*-E2 pathway (0cTS, −17.7 kcal mol$^{-1}$) exceed that of 0aRC by less than 1 kcal mol$^{-1}$. These results indicate that overcoming both barriers is easy. When the E2 reaction proceeds *via* a *syn*-E2 mechanism, the $HOO^-$ group abstracts the $H^\beta$ atom from the same side of leaving group I, and its transition state (0c′TS) is much greater in energy, with a value of −7.4 kcal mol$^{-1}$ with respect to the reactants. The halogen complex $[C_2H_5\cdots I\cdots OOH]^-$ (−19.0 kcal mol$^{-1}$) has a similar energy as 0aRC.

One water molecule is added to the $HOO^-$ anion to form $HO^-$(HOOH), and $HOO^-(H_2O)$ is 29.1 kcal mol$^{-1}$ exoergic. Starting from $HO^-$(HOOH) + $C_2H_5I$, the reaction energies of the $HOO^-$-$S_N2$, $HO^-$-$S_N2$, and E2 pathways are −36.4, −30.0, and −11.3 kcal mol$^{-1}$, respectively. The $HOO^-$-$S_N2$ and $HOO^-$-E2 pathways share the same RC, *i.e.*, 1aRC, and the $HO^-$-$S_N2$ (denoted as b) and $HO^-$-E2 pathways (denoted as d) share the same RC, denoted as 1bRC. The nomenclatures of TS and PC use the a, b, c, and d annotations. The pre-reaction complex for the $HO^-$ path (1bRC, −14.3 kcal mol$^{-1}$) is slightly more stable than that for the $HOO^-$ path (1aRC, −13.0 kcal mol$^{-1}$), as observed for the reaction with $CH_3Cl/CH_3I$.[32,54] Nevertheless, the transition states of the $HO^-$ paths are higher in energy than that for the $HOO^-$-path (either the $S_N2$ path or the E2 path). Arranged in ascending order of transition state energies, the order of pathways is $HOO^-$-$S_N2$ < $HO^-$-$S_N2$ < $HOO^-$-E2(*anti*) < $HO^-$-E2(*anti*). The energies are −9.4, −7.1, −6.2, and −4.0 kcal mol$^{-1}$ for 1aTS, 1bTS, 1cTS, and 1dTS, respectively.


© 2025 The Author(s). Published by the Royal Society of Chemistry

Open Access Article. Published on 24 July 2025. Downloaded on 8/11/2025 11:25:40 AM. This article is licensed under a Creative Commons Attribution-NonCommercial 3.0 Unported Licence.

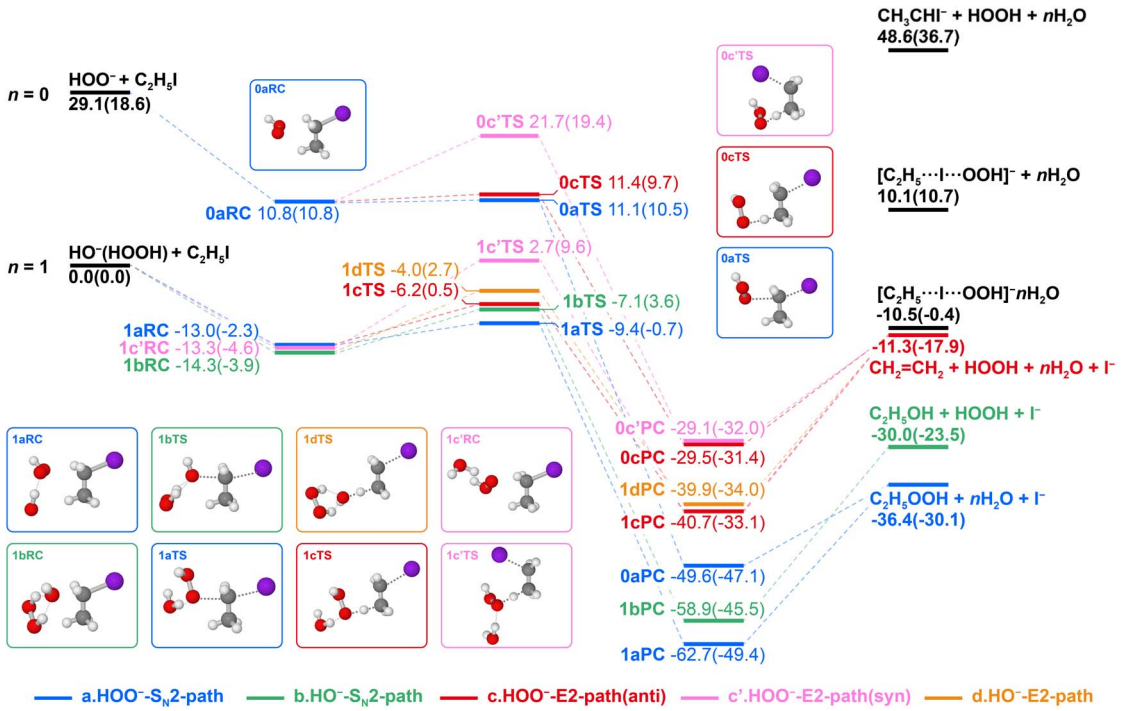


Fig. 3 Potential energy profile of $CH_3CH_2I$ reacting with $HOO^-$ and $HO^-(HOOH)$. (a) refers to the backside attack $HOO^-$-$S_N2$ pathway (blue); (b) refers to the backside attack $HO^-$-$S_N2$ pathway (green); (c) refers to the antisymmetric $HOO^-$-E2 pathway (red); (c′) refers to the *syn*-symmetric $HOO^-$-E2 pathway (pink); (d) refers to the antisymmetric $HO^-$-E2 pathway (orange). Energy values (in kcal $mol^{-1}$) excluding zero-point energy corrections are in normal text, and the values of Gibbs free energy at 298.15 K are in parentheses.

When the free energies are compared, the transition state of $HO^-$-$S_N2$ has the highest free energy among these four TSs. As expected, the *syn*-E2 path has an even higher transition state, 1c′TS, whose relative energy is 2.7 kcal $mol^{-1}$ in electronic energy and 9.6 kcal $mol^{-1}$ in free energy.

Assuming a Boltzmann distribution of these four pathways and according to the calculated free energies of the TSs, the thermal ratio at 300 K of $HOO^-$-$S_N2$ : $HOO^-$-E2 is 19.5 : 80.5 for the unsolvated system, and the thermal ratio of $HOO^-$-$S_N2$ : $HO^-$-$S_N2$ : $HOO^-$-E2 : $HO^-$-E2 is 87.9 : 0.1 : 11.7 : 0.3 for the singly solvated system. At an $E_{coll}$ of 0.04 eV, corresponding to a temperature of 300 K, the ratios given by direct dynamic simulations are 39.6 : 60.4 and 51.8 : 2.2 : 43.4 : 2.6. The thermal distribution predictions (based on stationary point calculations) and dynamic simulation results are consistent in that the $HOO^-$-E2 path is dominant under unsolvated conditions, whereas the $HOO^-$-$S_N2$ path is dominant under singly solvated conditions. Notably, the simulations provide a much higher percentage of the $HOO^-$-E2 path, differing by 20–30%, and a slightly higher percentage of the $HO^-$ paths. These results highlighted the dynamic characteristics of the reaction process. The dynamic preference of the E2 product channel has also been observed in the $F^-(CH_3OH)$ + $C_2H_5Br$ reaction,[4,5] where the dominant pathway given by simulation becomes the E2 path instead of the $S_N2$ path, which was predicted by the thermal distribution. The atomistic mechanisms discussed in the next section provide a detailed picture of the dynamic characteristics.

## Atomistic mechanisms

Different types of mechanisms were observed by tracking the animations of each reactive trajectory. The distribution of the mechanisms is shown in Fig. 4. The mechanisms are classified into direct and indirect mechanisms, depending on whether intermediates are formed during the trajectory.[20,65] For the unsolvated system, the reaction mechanism is primarily direct. At an $E_{coll}$ of 0.04 eV, the direct $HOO^-$-$S_N2$ mechanism accounts for 24.2%, and the direct $HOO^-$-E2 mechanism accounts for 40.4%; at an $E_{coll}$ of 1.0 eV, the corresponding values are 34.2% and 57.8%, respectively. As expected, a higher collision energy leads to more direct trajectories. For both the $HOO^-$-$S_N2$ and E2 pathways, both direct stripping (DS) and direct rebound (DR) mechanisms were observed, where the former is more common. The features of these mechanisms have been described in previous works,[20,65,66] and representative animations are presented in the ESI Movies.† The addition of one water molecule increases the percentage of indirect mechanisms. For the singly hydrated system, at an $E_{coll}$ of 0.04 eV, the indirect $HOO^-$-$S_N2$ mechanism accounts for 40.5%, and the indirect $HOO^-$-E2 mechanism accounts for 29.8%; at an $E_{coll}$ of 1.0 eV, the corresponding values are 22.2% and 21.8%, respectively. These values are much higher than the corresponding values from the unsolvated system, which are 15.4, 20.0, 3.1, and 4.9% (Fig. 4). The distributions of the product $I^-$ ion velocity scattering angle are shown in Fig. S2,† where the indirect mechanism shows isotropic scattering.

Open Access Article. Published on 24 July 2025. Downloaded on 8/11/2025 11:25:40 AM.
This article is licensed under a Creative Commons Attribution-NonCommercial 3.0 Unported Licence.

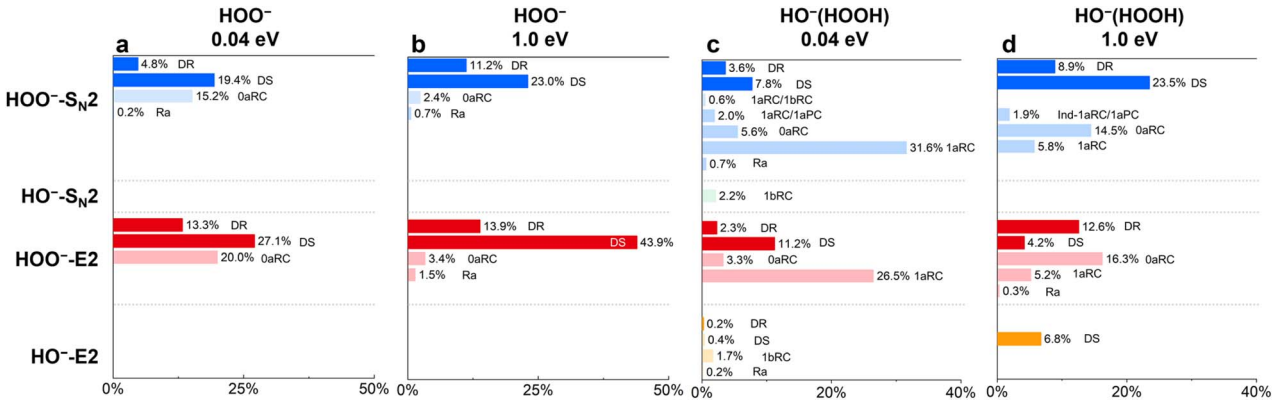


Fig. 4 Distributions of the reaction mechanisms for the $S_N2$ and E2 pathways for $CH_3CH_2I$ reacting with (a and b) $HOO^-$ and (c and d) $HO^-$(HOOH) at collision energies of 0.04 and 1.0 eV. Note: For unsolvated systems, the 0aRC mechanism involves α-elimination and $H^\alpha$-exchange mechanisms.

For both unsolvated and singly solvated systems, the observed indirect mechanisms include the formation of various intermediates and roundabout (Ra) mechanisms, where the latter contribute less than 3%. Previous reports of roundabout mechanisms of E2 reactions were limited to $F^-$ nucleophiles;[5,56,67,68] this work extends the roundabout mechanism to $HOO^-$ and $HO^-$(HOOH) reactions.

For both the $S_N2$ and E2 pathways, the dominant indirect mechanism is the formation of the $HOO^-\cdots C_2H_5I$ complex (0aRC) for the unsolvated system at both $E_{coll}$ values and the singly solvated system at an $E_{coll}$ of 1.0 eV. The dominant indirect mechanism becomes the formation of the $(H_2O)HOO^-\cdots C_2H_5I$ complex (1aRC) for the singly solvated system at an $E_{coll}$ of 0.04 eV. In addition, the mechanism of the singly solvated system was complicated by the participation of multiple intermediates, including 0aRC, 1aRC, 1bRC, and 1aPC. To demonstrate the indirect mechanisms, we provide snapshots of representative trajectories in Fig. 5. Fig. 5a shows an indirect $HOO^-$-$S_N2$ trajectory that is trapped in the pre-reaction complex 1aRC well for approximately 4 ps before the products are formed. Fig. 5c displays an indirect $HOO^-$-E2 trajectory that is trapped in the 1aRC well for ~9 ps. Then, the $HOO^-(H_2O)$ group abstracts the $H^\beta$ atom from the opposite side of leaving group I; specifically the *anti*-E2 mechanism occurs, and E2 products are formed. The lifetimes of pre-reaction complexes 1aRC were analysed by plotting $\ln[N(t)/N(0)]$ *versus* time ($t$) for the trajectories, where $N(0)$ refers to the number of trajectories that experienced the formation of RCs and $N(t)$ refers to the number of trajectories whose lifetimes of RCs are no less than $t$ (Fig. S3†). The resulting dissociation rate constant of 1aRC is 0.13 $ps^{-1}$ for the $S_N2$ path and 0.16 $ps^{-1}$ for the E2 path. Consequently, the corresponding half-lives of 1aRC are 5.33 and 4.33 ps; these results indicate that the reaction system was trapped in the pre-reaction complex well.

In addition to the *anti*-E2 mechanism, we also observed trajectories that follow the *syn*-E2 mechanism (Fig. S4b†). Owing to the higher transition states (Fig. 3) and greater steric hindrance than those of the *anti*-E2 paths, the *syn*-E2 trajectories constitute only a small portion of all E2 trajectories. For the unsolvated system, the fraction of *syn*-E2 trajectories is approximately 3% and 8% at $E_{coll}$ values of 0.04 and 1.0 eV; for the singly solvated system, the corresponding fractions are 0.9% and 0.

In the abovementioned *anti*-E2 and *syn*-E2 trajectories, the nucleophile first abstracts $H^\beta$ from the substrate $CH_3CH_2I$. For the unsolvated system at an $E_{coll}$ of 1.0 eV, the E2 trajectories may be initiated by a nucleophile abstracting a $H^\alpha$ atom. As shown in Fig. S5b,† $HOO^-$ initially abstracts an $H^\alpha$ atom from the $CH_3CH_2I$ substrate to form HOOH, followed by the C–I bond breaking, and then the substrate becomes $CH_3CH$. Thereafter, the substrate goes through an $H^\beta$-transfer transition state (EαTS) to generate $CH_2{=}CH_2$. This mechanism is called α-elimination (Eα) in previous simulations of $F^-$ + $CH_3CH_2Br$ reactions,[5] and this name is adopted here. The barrier of EαTS is as high as 7.9 kcal $mol^{-1}$ (Fig. S6†); thus, this mechanism is highly unfavourable and is observed only at an $E_{coll}$ of 1.0 eV and accounts for 2.2% of the $HOO^-$-E2 path.

In addition, the trajectories that experience the formation of 0aRC sometimes involve hydrogen exchange (HE) between the nucleophile $HOO^-$ and substrates, as observed in both the $S_N2$ and E2 pathways (Fig. S7b and S5c†). Similar to the first step of the Eα mechanism, the nucleophile initially abstracts an $H^\alpha$ atom from the $CH_3CH_2I$ substrate. The newly formed HOOH moiety transfers an H atom to $C^\alpha$ simultaneously or after a period, and then, the system reforms the $CH_3CH_2I$ and $HOO^-$ parts. This H-atom can be either the same $H^\alpha$ or the H that originally belonged to the nucleophile $HOO^-$. For the latter case, a transition state was located with a high barrier of 9.5 kcal $mol^{-1}$. Proton exchange may occur several times within a trajectory. These multiple types of hydrogen exchange trajectories are presented in Fig. S5 and S7.† Overall, these trajectories account for 0.36% (2.17%) of the $S_N2$ reactions and 0.63% (0.12%) of the E2 reactions at an $E_{coll}$ of 0.04 eV (1.0 eV). Notably, the $H^\alpha$-abstraction may generate $CH_3CHI^-$ + HOOH products. The product channel is 48.6 endothermic and was not observed during our simulation. However, a trace amount of $CH_3CHCl^-$ was observed in previous simulations of $F^-/HO^-$ + $CH_3CH_2Cl$.[69,70]


© 2025 The Author(s). Published by the Royal Society of Chemistry

Open Access Article. Published on 24 July 2025. Downloaded on 8/11/2025 11:25:40 AM. This article is licensed under a Creative Commons Attribution-NonCommercial 3.0 Unported Licence.

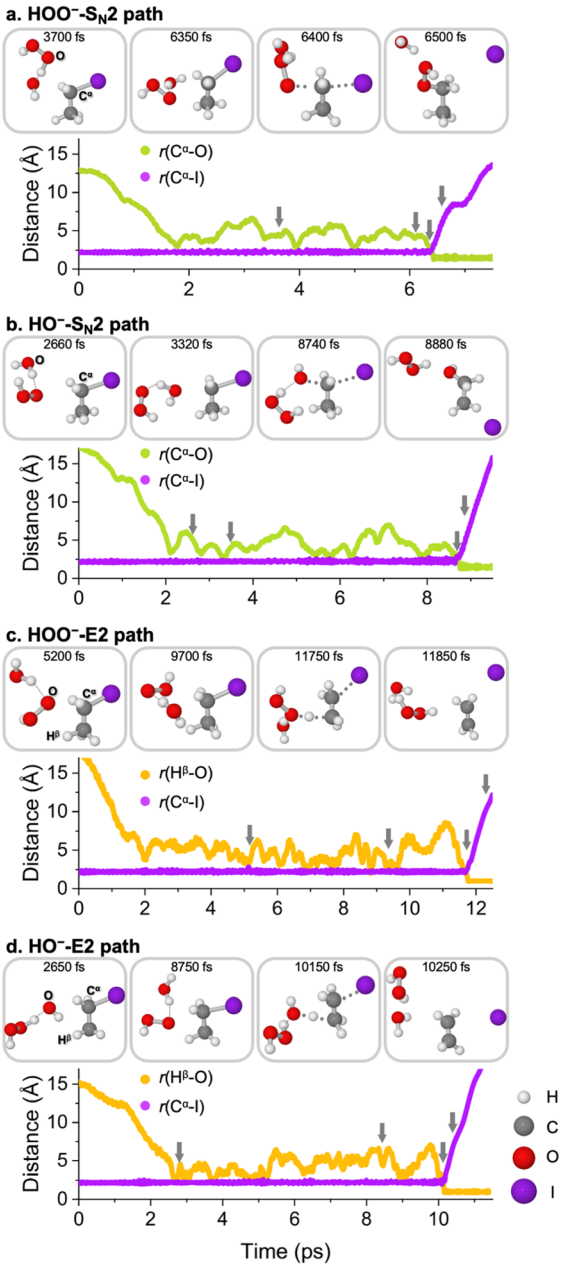


Fig. 5 Snapshots of the representative trajectories showing the indirect mechanism of the $HOO^-(H_2O)$ + $CH_3CH_2I$ reaction. The distance between the $C^\alpha$ atom and I atom $r(C^\alpha\text{-I})$ (purple), the distance between the $C^\alpha$ atom and the attacking O atom $r(C^\alpha\text{–O})$ (green), and the distance between $H^\beta$ and the attacking O atom $r(H^\beta\text{–O})$ (orange) are shown as a function of time. (a) $HOO^-$-$S_N2$ pathway, (b) $HO^-$-$S_N2$ pathway, (c) $HOO^-$-E2 pathway, (d) $HO^-$-E2 pathway.

Interestingly, these α-elimination and $H^\alpha$-exchange mechanisms were not observed in the singly hydrated system. This can be understood by comparing the proton affinities (PAs). The PA of $HOO^-$ is 375.9 kcal $mol^{-1}$, and the PA of $HO^-$(HOOH) is 357.0 kcal mol; thus, the abstraction of either $H^\alpha$ or $H^\beta$ from $CH_3CH_2I$ by $HO^-$(HOOH) is more difficult than that by $HOO^-$. Instead, the proton transfer between the nucleophiles and substrates is completely suppressed by proton transfer within the singly solvated nucleophile $HO^-$(HOOH). Representative trajectory snapshots are shown in Fig. S8 and S9.†

For the water-induced $HO^-$-$S_N2$ and $HO^-$-E2 pathways, Fig. 5b and d show that these trajectories also experience a long time (approximately 6–7 ps) within the pre-reaction complex well; here, the nucleophile group strongly interconverts between $HOO^-(H_2O)$ and $HO^-$(HOOH). The singly solvated pre-reaction complexes $(H_2O)HOO^-\cdots C_2H_5I$ (1aRC) and (HOOH) $HO^-\cdots C_2H_5I$ (1bRC) are close in energy, and the latter is approximately 1 kcal $mol^{-1}$ more stable. However, tracking the trajectories within the well indicates that the system prefers to stay in the configuration of $(H_2O)HOO^-\cdots C_2H_5I$. For example, for a representative $HO^-$-$S_N2$ trajectory (Fig. 5b) and considering the time within the pre-reaction complex well, the system adopts the $(H_2O)HOO^-\cdots C_2H_5I$ configuration 69% of the time, and this value is 73% for a representative $HO^-$-E2 trajectory (Fig. 5d). The more stable $(HOOH)HO^-\cdots C_2H_5I$ configuration only accounts for 31% and 27%, respectively. A detailed analysis is provided in Fig. S10.† This occurs because the symmetric structure of $(HOOH)HO^-$ in 1bRC can easily be disturbed during the dynamic reaction process, namely, the entropy effect. Hence, the lower probability of the $HO^-$ configurations within the well and the higher barrier both lead to the suppression of the $HO^-$ paths, both $S_N2$ and E2. Nevertheless, the simulated $HO^-$ paths have a slightly greater portion than those predicted by the thermal distribution at 300 K; these results indicate the dynamic effects of proton transfer during the reaction processes.

Finally, we investigated the reason for the suppression of the thermodynamically favoured solvated product $I^-$(solvent) by the $I^-$ product from the simulation. To understand this, we plotted the time at which the $H_2O$ molecule departed from the system against the formation time of $CH_3CH_2OOH$ for the $HOO^-$-$S_N2$ pathway and against the formation time of $CH_2{=}CH_2$ for the $HOO^-$-E2 pathway (Fig. 6). At $E_{coll}$ = 0.04 eV, the formation of

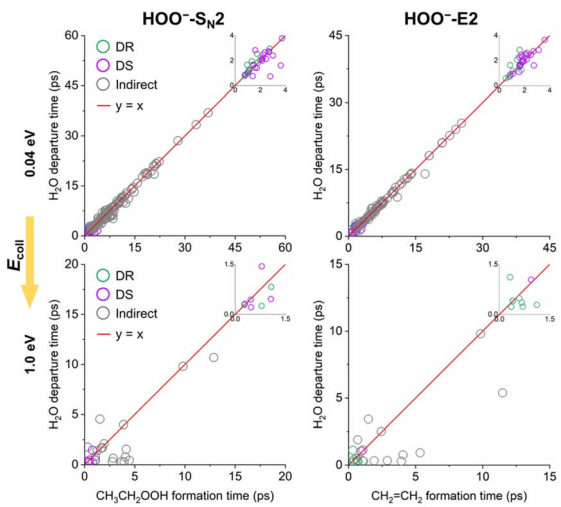


Fig. 6 Water-leaving time as a function of $CH_3CH_2OOH$ (left) and $CH_2{=}CH_2$ (right) formation time for the $HOO^-(H_2O)$ + $CH_3CH_2I$ reaction at 0.04 (top) and 1.0 eV (bottom) collision energies.

Open Access Article. Published on 24 July 2025. Downloaded on 8/11/2025 11:25:40 AM. This article is licensed under a Creative Commons Attribution-NonCommercial 3.0 Unported Licence.

$CH_3CH_2OOH$ or $CH_2{=}CH_2$ simultaneously occurred with the departure of $H_2O$, mostly within 20 ps. As $E_{coll}$ increased to 1.0 eV, the majority of $S_N2$ reactions occurred within 5 ps, whereas the $H_2O$ molecules were removed much earlier, mainly before 2.5 ps. Similarly, the E2 reactions occurred within ~4 ps, and the $H_2O$ molecules were removed before 2.0 ps. With a time width of ±250 fs centred on the unit slope line, the percentages of the trajectories for $S_N2$ and E2 were 65.2% and 71.5%, respectively, at $E_{coll}$ = 0.04 eV, and the corresponding values decreased to 46.0% and 41.4%, respectively, at $E_{coll}$ = 1.0 eV. The above analysis, together with the mechanism analysis, indicated that a large portion of the collision energy and/or the reaction exothermicity were transferred to the relative translational energy of the solvent and the remaining parts. Consequently, solvated products were rarely observed.

## Conclusions

In this work, the effect of a single water molecule on the reaction between the hydroperoxide anion and ethyl iodide was investigated by direct dynamics simulation. The introduction of one water molecule had multiple effects. First, it lowered the overall reactivity; here, the rate constant was reduced by 61% and 63% in comparison to that of the solvent-free reaction, under the considered collision energies of 0.04 and 1.0 eV. Second, it changed the preference between the competing $S_N2$ and E2 reactions. The $S_N2$-to-E2 ratio was approximately 40 : 60 for the solvent-free system, and this ratio changed to approximately 54 : 46 for the single-solvation system under both $E_{coll}$ values. A single solvent shifted the preference from E2 to $S_N2$ because of the differential solvation effect that led to a higher barrier for the E2 path than for the $S_N2$ path. However, the dynamical simulations resulted in more E2 trajectories than what was predicted by the potential energy profiles. Increasing $E_{coll}$ did not affect the $S_N2$-to-E2 ratio but lowered the overall reactivity by 82%.

Third, the extra water molecules facilitated new pathways *via* proton transfer between $HOO^-(H_2O)$ and $HO^-(HOOH)$, thus leading to the $HO^-$-$S_N2$ and $HO^-$-E2 paths, in addition to the traditional $HOO^-$-$S_N2$ and $HOO^-$-E2 paths, where the latter two paths were dominant. The percentages of $HOO^-$-$S_N2$, $HOO^-$-E2, $HO^-$-$S_N2$, and $HO^-$-E2 paths were 51.8%, 43.4%, 2.2%, and 2.6%, respectively, at an $E_{coll}$ of 0.04 eV and 54.6%, 38.6%, 0, and 6.8%, respectively, at an $E_{coll}$ of 1.0 eV. Extensive proton transfer within the pre-reaction complex well drove the occurrence of the $HO^-$ paths. However, the lower probability of $HO^-$ configurations that caused by the entropy effect and the relatively higher barrier led to their low percentages. We anticipate that the solvent molecule inducing new pathways is not an isolated case, especially for protic solvents such as $H_2O$, $NH_3$, and $CH_3OH$. However, such studies are quite limited so far. Singly-solvated anions like $OH^-(H_2O)$, $NH_2^-(NH_3)$, and $CH_3O^-(CH_3OH)$ experience extensive proton exchange, but generate the same type of anions. Anions like $F^-(H_2O)$, $HO^-(NH_3)$, $HOO^-(NH_3)$, and $CH_3O^-(H_2O)$ can generate new nucleophiles through proton transfer, but they are usually higher in energy. Their dynamics remain to be explored in the future.

Fourth, the introduction of one water molecule complicated the reaction mechanisms, increased the percentage of indirect mechanism, and affected the dynamical feature of proton transfer. For the solvent-free system, proton transfer occurred between nucleophiles and substrates; for example, α-elimination and $H^\alpha$-exchange mechanisms were observed. In contrast, for the singly solvated system, proton transfer mainly occurred within the nucleophile, *i.e.*, the configurations shifted between $(H_2O)HOO^-\cdots C_2H_5I$ and $(HOOH)HO^-\cdots C_2H_5I$. Finally, solvated products were observed for the singly solvated reactions, but at a very low percentage of 3%. This occurred because a large portion of the collision energy and/or the reaction exothermicity were transferred to the translation of the products.

To conclude, this work revealed that for the $HOO^- + C_2H_5I$ reaction, a single water molecule affected more than the reactivity and competition between the $S_N2$ and E2 reactions. It also induced new competing pathways that used $HO^-$ as an attacking nucleophile *via* proton transfer and complicated the reaction mechanisms. These dynamic roles of the individual solvent molecules observed in this work could reveal new facets of reaction dynamics relevant to organic synthesis, biochemistry,[71,72] microdroplet chemistry,[73–76] and chemistry in aerosols.[77–80]

## Data availability

Data are in ESI.†

## Author contributions

J. X. designed the research. X. Wu performed the computations, analyzed the data, prepared the figures and tables, and wrote the draft of the paper. C. Z. edited the paper. J. X. and J. S. F. supervised the research and edited the paper.

## Conflicts of interest

There are no conflicts to declare.

## Acknowledgements

This work was supported by the National Key Research and Development Program of China (2024YFA1509602), the National Natural Science Foundation of China (no. 22273004), and the Teli Fellowship and the Innovation Foundation (no. 2021CX01026) from the Beijing Institute of Technology, China.

## References

1 E. Vöhringer-Martinez, B. Hansmann, H. Hernandez, J. S. Francisco, J. Troe and B. Abel, *Science*, 2007, **315**, 497–501.
2 G. I. Almerindo and J. R. Pliego, *Chem. Phys. Lett.*, 2006, **423**, 459–462.
3 X. Liu, J. Xie, J. Zhang, L. Yang and W. L. Hase, *J. Phys. Chem. Lett.*, 2017, **8**, 1885–1892.

 © 2025 The Author(s). Published by the Royal Society of Chemistry

Open Access Article. Published on 24 July 2025. Downloaded on 8/11/2025 11:25:40 AM. This article is licensed under a Creative Commons Attribution-NonCommercial 3.0 Unported Licence.

4 X. Liu, J. Zhang, L. Yang and W. L. Hase, *J. Am. Chem. Soc.*, 2018, **140**, 10995–11005.
5 H. Wang, X. Liu, S. Zhao, G. Fu, W. Zhen, L. Yang and J. Zhang, *Precis. Chem.*, 2024, **2**, 40–48.
6 D. K. Bohme and G. I. Mackay, *J. Am. Chem. Soc.*, 1981, **103**, 978–979.
7 F. M. Bickelhaupt, E. J. Baerends and N. M. M. Nibbering, *Chem.–Eur. J.*, 1996, **2**, 196–207.
8 N. Eyet, J. J. Melko, S. G. Ard and A. A. Viggiano, *Int. J. Mass Spectrom.*, 2015, **378**, 54–58.
9 T. Hansen, J. C. Roozee, F. M. Bickelhaupt and T. A. Hamlin, *J. Org. Chem.*, 2022, **87**, 1805–1813.
10 R. Otto, J. Brox, S. Trippel, M. Stei, T. Best and R. Wester, *Nat. Chem.*, 2012, **4**, 534–538.
11 L. Yang, X. Liu, J. Zhang and J. Xie, *Phys. Chem. Chem. Phys.*, 2017, **19**, 9992–9999.
12 K. Doi, E. Togano, S. S. Xantheas, R. Nakanishi, T. Nagata, T. Ebata and Y. Inokuchi, *Angew. Chem., Int. Ed.*, 2013, **52**, 4380–4383.
13 C. Zhu, X. C. Zeng, J. S. Francisco and I. Gladich, *J. Am. Chem. Soc.*, 2020, **142**, 5574–5582.
14 B. Tang, Q. Bai, Y.-G. Fang, J. S. Francisco, C. Zhu and W.-H. Fang, *J. Am. Chem. Soc.*, 2024, **146**, 21742–21751.
15 Y.-G. Fang, L. Wei, J. S. Francisco, C. Zhu and W.-H. Fang, *J. Am. Chem. Soc.*, 2024, **146**, 21052–21060.
16 Z. Wan, C. Zhu and J. S. Francisco, *J. Am. Chem. Soc.*, 2023, **145**, 17478–17484.
17 Z. Wan, Y. Fang, Z. Liu, J. S. Francisco and C. Zhu, *J. Am. Chem. Soc.*, 2023, **145**, 944–952.
18 G. T. Dunning, D. R. Glowacki, T. J. Preston, S. J. Greaves, G. M. Greetham, I. P. Clark, M. Towrie, J. N. Harvey and A. J. Orr-Ewing, *Science*, 2015, **347**, 530–533.
19 F. Xie, D. S. Tikhonov and M. Schnell, *Science*, 2024, **384**, 1435–1440.
20 J. Xie, R. Otto, J. Mikosch, J. Zhang, R. Wester and W. L. Hase, *Acc. Chem. Res.*, 2014, **47**, 2960–2969.
21 R. Otto, J. Xie, J. Brox, S. Trippel, M. Stei, T. Best, M. R. Siebert, W. L. Hase and R. Wester, *Faraday Discuss.*, 2012, **157**, 41–57.
22 R. Otto, J. Brox, S. Trippel, M. Stei, T. Best and R. Wester, *J. Phys. Chem. A*, 2013, **117**, 8139–8144.
23 B. Bastian, T. Michaelsen, L. Li, M. Ončák, J. Meyer, D. H. Zhang and R. Wester, *J. Phys. Chem. A*, 2020, **124**, 1929–1939.
24 B. Bastian, T. Michaelsen, M. Ončák, J. Meyer and R. Wester, *Int. J. Mass Spectrom.*, 2021, **462**, 116526.
25 X. Lu, L. Li, X. Zhang, B. Fu, X. Xu and D. H. Zhang, *J. Phys. Chem. Lett.*, 2022, **13**, 5253–5259.
26 X. Lu, C. Shang, L. Li, R. Chen, B. Fu, X. Xu and D. H. Zhang, *Nat. Commun.*, 2022, **13**, 4427.
27 D. A. Tasi and G. Czakó, *Chem. Sci.*, 2021, **12**, 14369–14375.
28 Y. Feng, L. Zhou, Q. Wan, S. Lin and H. Guo, *Chem. Sci.*, 2018, **9**, 5890–5896.
29 R. Yin, B. Jiang and H. Guo, *ACS Catal.*, 2022, **12**, 6486–6494.
30 J. Xie, R. Otto, R. Wester and W. L. Hase, *J. Chem. Phys.*, 2015, **142**, 244308.
31 J. Xie, X. Ma, J. Zhang, P. M. Hierl, A. A. Viggiano and W. L. Hase, *Int. J. Mass Spectrom.*, 2017, **418**, 122–129.
32 C. Zhao, X. Ma, X. Wu, D. L. Thomsen, V. M. Bierbaum and J. Xie, *J. Phys. Chem. Lett.*, 2021, **12**, 7134–7139.
33 M. A. Vincent, I. J. Palmer, I. H. Hillier and E. Akhmatskaya, *J. Am. Chem. Soc.*, 1998, **120**, 3431–3439.
34 J. A. Cotruvo, Jr. and J. Stubbe, *Biochemistry*, 2010, **49**, 1297–1309.
35 L. Q. Tuan, H. Umakoshi, T. Shimanouchi and R. Kuboi, *Enzyme Microb. Technol.*, 2009, **44**, 101–106.
36 M. A. Babizhayev, K. S. Vishnyakova and Y. E. Yegorov, *Fundam. Clin. Pharmacol.*, 2011, **25**, 139–162.
37 L. Qiao, Y. Lu, B. Liu and H. H. Girault, *J. Am. Chem. Soc.*, 2011, **133**, 19823–19831.
38 H. Wang, Z. Song, W. Liu and H. Kong, *Microelectron. Eng.*, 2011, **88**, 1010–1015.
39 S. Siddiqui, M. Keswani, B. Brooks, A. Fuerst and S. Raghavan, *Microelectron. Eng.*, 2013, **102**, 68–73.
40 S. H. Zeronian and M. K. Inglesby, *Cellulose*, 1995, **2**, 265–272.
41 S. W. Benson and P. S. Nangia, *Acc. Chem. Res.*, 1979, **12**, 223–228.
42 A. B. Fialkov, *Prog. Energy Combust. Sci.*, 1997, **23**, 399–528.
43 Y. Qiao, S. Wu, J. Yi, Y. Sun, S. Guo, S. Yang, P. He and H. Zhou, *Angew. Chem., Int. Ed.*, 2017, **56**, 4960–4964.
44 Z. Ma, D. Anick and M. E. Tuckerman, *J. Phys. Chem. B*, 2014, **118**, 7937–7945.
45 D. L. Thomsen, J. N. Reece, C. M. Nichols, S. Hammerum and V. M. Bierbaum, *J. Am. Chem. Soc.*, 2013, **135**, 15508–15514.
46 D. L. Thomsen, C. M. Nichols, J. N. Reece, S. Hammerum and V. M. Bierbaum, *J. Am. Soc. Mass Spectrom.*, 2014, **25**, 159–168.
47 D. L. Thomsen, J. N. Reece, C. M. Nichols, S. Hammerum and V. M. Bierbaum, *J. Phys. Chem. A*, 2014, **118**, 8060–8066.
48 D. J. Anick, *J. Phys. Chem. A*, 2011, **115**, 6327–6338.
49 F. Yu, *J. Chem. Phys.*, 2018, **148**, 014302.
50 Z. Kerekes, D. A. Tasi and G. Czakó, *J. Phys. Chem. A*, 2022, **126**, 889–900.
51 A. Gutal and M. Paranjothy, *Phys. Chem. Chem. Phys.*, 2023, **25**, 15015–15022.
52 X. Liu, S. Tian, B. Pang, H. Li and Y. Wu, *Phys. Chem. Chem. Phys.*, 2023, **25**, 14812–14821.
53 X. Liu, W. Guo, H. Feng, B. Pang and Y. Wu, *J. Phys. Chem. A*, 2023, **127**, 7373–7382.
54 X. Wu, C. Zhao, S. Zhang and J. Xie, *J. Phys. Chem. A*, 2024, **128**, 2393–2398.
55 X. Wu, C. Zhao and J. Xie, *ChemPhysChem*, 2022, **23**, e202200285.
56 E. Carrascosa, J. Meyer, J. Zhang, M. Stei, T. Michaelsen, W. L. Hase, L. Yang and R. Wester, *Nat. Commun.*, 2017, **8**, 25.
57 L. Yang, J. Zhang, J. Xie, X. Ma, L. Zhang, C. Zhao and W. L. Hase, *J. Phys. Chem. A*, 2017, **121**, 1078–1085.
58 X. Wu, S. Zhang and J. Xie, *Phys. Chem. Chem. Phys.*, 2022, **24**, 12993–13005.

Open Access Article. Published on 24 July 2025. Downloaded on 8/11/2025 11:25:40 AM.
This article is licensed under a Creative Commons Attribution-NonCommercial 3.0 Unported Licence.

59 X. Wu, F. M. Bickelhaupt and J. Xie, *Phys. Chem. Chem. Phys.*, 2024, **26**, 11320–11330.
60 W. L. Hase, R. J. Duchovic, X. Hu, A. Komornicki, K. F. Lim, D. H. Lu, G. H. Peslherbe, K. N. Swamy, S. R. V. Linde, A. J. C. Varandas, H. Wang and R. J. Wolf, *Quantum Chem. Program Exch. Bull*, 1996, **16**, 671.
61 M. Valiev, E. J. Bylaska, N. Govind, K. Kowalski, T. P. Straatsma, H. J. J. Van Dam, D. Wang, J. Nieplocha, E. Apra, T. L. Windus and W. A. de Jong, *Comput. Phys. Commun.*, 2010, **181**, 1477–1489.
62 U. Lourderaj, R. Sun, S. C. Kohale, G. L. Barnes, W. A. de Jong, T. L. Windus and W. L. Hase, *Comput. Phys. Commun.*, 2014, **185**, 1074–1080.
63 L. Verlet, *Phys. Rev.*, 1967, **159**, 98–103.
64 J. Zhang, L. Yang, J. Xie and W. L. Hase, *J. Phys. Chem. Lett.*, 2016, **7**, 660–665.
65 J. Xie and W. L. Hase, *Science*, 2016, **352**, 32–33.
66 J. Zhang, J. Mikosch, S. Trippel, R. Otto, M. Weidemüller, R. Wester and W. L. Hase, *J. Phys. Chem. Lett.*, 2010, **1**, 2747–2752.
67 S. Zhao, H. Wang, G. Fu, W. Zhen, M. Liu, L. Yang and J. Zhang, *Precis. Chem.*, 2023, **1**, 507–515.
68 X. Wu, F. Ying, H. Wang, L. Yang, J. Zhang and J. Xie, *ACS Phys. Chem. Au*, 2024, **4**, 581–592.
69 J. Meyer, V. Tajti, E. Carrascosa, T. Győri, M. Stei, T. Michaelsen, B. Bastian, G. Czakó and R. Wester, *Nat. Chem.*, 2021, **13**, 977–981.
70 A. B. Nacsa, C. Tokaji and G. Czakó, *Faraday Discuss.*, 2024, **251**, 604–621.
71 D. R. B. Brittain, R. Pandey, K. Kumari, P. Sharma, G. Pandey, R. Lal, M. L. Coote, J. G. Oakeshott and C. J. Jackson, *Chem. Commun.*, 2011, **47**, 976–978.
72 D. O'Hagan and J. W. Schmidberger, *Nat. Prod. Rep.*, 2010, **27**, 900–918.
73 X. Yan, R. M. Bain and R. G. Cooks, *Angew. Chem., Int. Ed.*, 2016, **55**, 12960–12972.
74 S. Banerjee, E. Gnanamani, X. Yan and R. N. Zare, *Analyst*, 2017, **142**, 1399–1402.
75 K. Li, K. Gong, J. Liu, L. Ohnoutek, J. Ao, Y. Liu, X. Chen, G. Xu, X. Ruan, H. Cheng, J. Han, G. Sui, M. Ji, V. K. Valev and L. Zhang, *Cell Rep. Phys. Sci.*, 2022, **3**, 100917.
76 S. Jin, H. Chen, X. Yuan, D. Xing, R. Wang, L. Zhao, D. Zhang, C. Gong, C. Zhu, X. Gao, Y. Chen and X. Zhang, *JACS Au*, 2023, **3**, 1563–1571.
77 J. Li, N. T. Tsona and L. Du, *Phys. Chem. Chem. Phys.*, 2018, **20**, 10650–10659.
78 N. Tsona Tchinda, L. Du, L. Liu and X. Zhang, *Atmos. Chem. Phys.*, 2022, **22**, 1951–1963.
79 Y. Liu, Q. Ge, T. Wang, R. Zhang, K. Li, K. Gong, L. Xie, W. Wang, L. Wang, W. You, X. Ruan, Z. Shi, J. Han, R. Wang, H. Fu, J. Chen, C. K. Chan and L. Zhang, *Chem*, 2024, **10**, 330–351.
80 J. Liu, Y. Zhao, X. Lian, D. Li, X. Zhang, J. Chen, B. Deng, X. Lan and Y. Shao, *Molecules*, 2024, **29**, 4033.


© 2025 The Author(s). Published by the Royal Society of Chemistry